Research Article | Vol. 25, No. 4 | 20 Feb 2017 | OPTICS EXPRESS 4268

Optics EXPRESS

Ultra-broadband two-pump optical parametric amplifier in tellurite waveguides with engineered dispersion

JORGE D. MARCONI,[1,*] MARCELO L. F. ABBADE,[2] CLAUDIA M. SERPA-IMBETT,[3] AND ERIC A. M. FAGOTTO[4]

[1]*Centro de Engenharia, Modelagem e Ciências Sociais Aplicadas, Universidade Federal do ABC, UFABC, SP, Brazil*
[2]*São Paulo State University (UNESP),Campus of São João da Boa Vista, SP, Brazil*
[3]*School of Electrical Engineering and Computer Science, Unicamp, Campinas, SP, Brazil*
[4]*School of Electrical Engineering, PUC-Campinas, Campinas, SP, Brazil*
[*]*jorge.marconi@ufabc.edu.br*

Abstract: The capacity of communication networks may be significantly improved by simply enhancing the optical amplifier bandwidth. This paper presents a numerical investigation of an ultra-broadband, low-ripple, two-pump-optical parametric amplifier (2P-OPA) that employs a tellurite glass buried-channel type nano-waveguide as nonlinear medium. The nano-waveguide was designed as a 25-cm-long Archimedean spiral that occupies a footprint of only ~2.5 mm^2, with a ~0.7 μm^2 effective cross section. Its zero-dispersion wavelength is ~1550 nm, the nonlinear coefficient is ~3000 W^{-1} km^{-1}, and the attenuation coefficient is ~0.5 dB/m (1100 to 1900 nm). Simulations suggest a 2P-OPA based on such waveguide will be able to amplify 243 QPSK input channels modulated at 56 Gbps over 102 nm bandwidth, over metropolitan area network scales.

OCIS codes: (190.0190) Nonlinear optics; (190.4970) Parametric oscillators and amplifiers; (130.0130) Integrated optics; (130.3120) Integrated optics devices; (130.4310) Nonlinear.

References and links

1. P. Bayvel, R. Maher, T. Xu, G. Liga, N. A. Shevchenko, D. Lavery, A. Alvarado, and R. I. Killey, "Maximizing the optical network capacity," Phil. Trans. R. Soc. A **374**(2062), 20140440 (2016).
2. A. D. Ellis, N. M. Suibhne, D. Saad, and D. N. Payne, "Communication networks beyond the capacity crunch," Phil. Trans. R. Soc. A **374**(2062), 20150191 (2016).
3. J. X. Cai, Y. Sun, H. Zhang, H. G. Batshon, M. V. Mazurczyk, O. V. Sinkin, D. G. Foursa, and A. Pilipetskii, "49.3 Tb/s transmission over 9100 km using C+L EDFA and 54 Tb/s transmission over 9150 km using hybrid-Raman EDFA," J. Lightwave Technol. **33**(15), 2724–2734 (2015).
4. R. J. Essiambre and R. W. Tkach, "Capacity trend and limits of optical communication networks," Proc. IEEE **100**(5), 1035–1055 (2012).
5. R. J. Essiambre, G. J. Foschini, G. Kramer, and P. J. Winzer, "Capacity limits of information transmission in optically-routed fiber networks," Bell Labs Tech. J. **14**(4), 149–162 (2010).
6. R. J. Essiambre, G. Kramer, P. J. Winzer, G. J. Foschini, and B. Goebel, "Capacity limits of optical fiber networks," J. Lightwave Technol. **28**(4), 662–701 (2010).
7. J. Berthold, A. A. M. Saleh, L. Blair, and J. M. Simmons, "Optical networking: past, present, and future," J. Lightwave Technol. **26**(9), 1104–1118 (2008).
8. E. B. Desurvire, "Capacity demand and technology challenges for lightwave systems in the next two decades," J. Lightwave Technol. **24**(12), 4697–4710 (2006).
9. D. C. Kilper and H. Rastegarfar, "Energy challenges in optical access and aggregation networks," Phil. Trans. R. Soc. A **374**(2062), 20140435 (2016).
10. S. Beppu, K. Kasai, M. Yoshida, and M. Nakazawa, "2048 QAM (66 Gbit/s) single-carrier coherent optical transmission over 150 km with a potential SE of 15.3 bit/s/Hz," Opt. Express **23**(4), 4960–4969 (2015).
11. J. Sakaguchi, W. Klaus, J. M. D. Mendinueta, B. J. Puttnam, R. S. Luís, Y. Awaji, N. Wada, T. Hayashi, T. Nakanishi, T. Watanabe, Y. Kokubun, T. Takahata, and T. Kobayashi, "Large spatial channel (36-core x 3 mode) heterogeneous few-mode multicore fiber," J. Lightwave Technol. **34**(1), 93–103 (2016).
12. F. Poletti, M. N. Petrovich, and D. J. Richardson, "Hollow-core photonic bandgap fibers: technology and applications," Nanophotonics **2**(5–6), 315–340 (2013).

#279786 https://doi.org/10.1364/OE.25.004268
Journal © 2017 Received 31 Oct 2016; revised 31 Jan 2017; accepted 1 Feb 2017; published 16 Feb 2017

Optics EXPRESS

13. J. M. Chavez Boggio, A. Guimarães, F. A. Callegari, J. D. Marconi, and H. L. Fragnito, "Q penalties due to pump phase modulation and pump RIN in fiber optic parametric amplifiers with non-uniform dispersion," Opt. Commun. **249**(4–6), 451–472 (2005).
14. J. M. Chavez Boggio, J. D. Marconi, S. R. Bickham, and H. L. Fragnito, "Spectrally flat and broadband double-pumped fiber optical parametric amplifiers," Opt. Express **15**(9), 5288–5309 (2007).
15. L. Zhang, T.-H. Tuan, H. Kawamura, K. Nagasaka, T. Suzuki, and Y. Ohishi, "Broadband optical parametric amplifier formed by two pairs of adjacent four-wave mixing sidebands in a tellurite microstructured optical fibre," J. Opt. **18**(5), 055502 (2016).
16. P. S. Maji and P. R. Chaudhuri, "Gain and bandwidth investigation in a near-zero ultra-flat dispersion PCF for optical parametric amplification around the communication wavelength," Appl. Opt. **54**(11), 3263–3272 (2015).
17. D. Bigourd, P. B. d'Augerès, J. Dubertrand, E. Hugonnot, and A. Mussot, "Ultra-broadband fiber optical parametric amplifier pumped by chirped pulses," Opt. Lett. **39**(13), 3782–3785 (2014).
18. S. K. Chatterjee, S. N. Khan, and P. R. Chaudhuri, "Two-octave spanning single pump parametric amplification at 1550 nm in a host lead-silicate binary multi-clad microstructure fiber: influence of multi-order dispersion engineering," Opt. Commun. **332**, 244–256 (2014).
19. M. W. Lee, T. Sylvestre, M. Delqué, A. Kudlinski, A. Mussot, J.-F. Gleyze, A. Jolly, and H. Maillotte, "Demonstration of an all-fiber broadband optical parametric amplifier at 1 μm," J. Lightwave Technol. **28**(15), 2173–2178 (2010).
20. J. M. Chavez Boggio, S. Moro, E. Myslivets, J. R. Windmiller, N. Alic, and S. Radic, "155-nm continuous-wave two-pump parametric amplification," IEEE Photonics Technol. Lett. **21**(10), 612–614 (2009).
21. T. Toroundinis and P. Andrekson, "Broadband single-pumped fiber-optic parametric amplifiers," IEEE Photonics Technol. Lett. **19**(9), 650–652 (2007).
22. H. Hu, R. M. Jopson, A. H. Gnauck, M. Dinu, S. Chandrasekhar, C. Xie, and S. Randel, "Parametric amplification, wavelength conversion, and phase conjugation of a 2048-Tbit/;s WDM PDM 16-QAM signal," J. Lightwave Technol. **33**(7), 1286–1291 (2015).
23. N. El Dahdah, D. S. Govan, M. Jamshidifar, N. J. Doran, and M. E. Marhic, "Fiber optical parametric amplifier performance in a 1-Tb/s DWDM communication system," IEEE J. Sel. Top. Quantum Electron. **18**(2), 950–957 (2012).
24. X. Liu, R. M. Osgood Jr., Y. A. Vlasov, and W. M. J. Green, "Mid-infrared optical parametric amplifier using silicon nanophotonic waveguides," Nat. Photonics **4**, 557–560 (2010).
25. M. A. Foster, A. C. Turner, J. E. Sharping, B. S. Schmidt, M. Lipson, and A. L. Gaeta, "Broad-band optical parametric gain on a silicon photonic chip," Nature **441**(7096), 960–963 (2006).
26. A. Pasquazi, Y. Park, J. Azaña, F. Légaré, R. Morandotti, B. E. Little, S. T. Chu, and D. J. Moss, "Efficient wavelength conversion and net parametric gain via four wave mixing in a high index doped silica waveguide," Opt. Express **18**(8), 7634–7641 (2010).
27. J. J. Leal, R. Narro-Garcia, H. Desirena, J. D. Marconi, E. Rodrigues, K. Linganna, and E. De la Rosa, "Spectroscopic properties of tellurite glasses co-doped with Er3+ and Yb3+," J. Lumin. **162**(13195), 72–80 (2015).
28. K. S. Bindra, H. T. Bookey, A. K. Kar, B. S. Wherrett, X. Liu, and A. Jha, "Nonlinear optical properties of chalcogenide glasses: Observation of multiphoton absorption," Appl. Phys. Lett. **79**(13), 1939–1941 (2001).
29. S. Shen, A. Jha, X. Liu, M. Nafataly, K. Bindra, H. J. Bookey, and A. K. Kar, "Tellurite glasses for broadband amplifiers and integrated optics," J. Am. Ceram. Soc. **85**(6), 1391–1395 (2002).
30. A. Jha, *Inorganic Glasses for Photonics* (John Wiley & Sons, 2016), Chap. 7.
31. M. E. Marhic, *Fiber Optical Parametric Amplifiers, Oscillators, and Related Devices* (Cambridge University, 2007), Ch. 3.
32. X. Guan, Y. Ding, and L. H. Frandsen, "Ultra-compact broadband higher order-mode pass filter fabricated in a silicon waveguide for multimode photonics," Opt. Lett. **40**(16), 3893–3896 (2015).
33. S. Khan, J. Chiles, J. Ma, and S. Fathpour, "Silicon-on-nitride waveguides for mid-and near- infrared integrated photonics," Appl. Phys. Lett. **102**(12), 121104 (2013).
34. C. Schulze, D. Flamm, S. Unger, S. Schröter, and M. Duparré, "Measurement of higher-order mode propagation losses in effectively single mode fibers," Opt. Lett. **38**(23), 4958–4961 (2013).
35. Y. Jung, Y. Jeong, G. Brambilla, and D. J. Richardson, "Adiabatically tapered splice for selective excitation of the fundamental mode in a multimode fiber," Opt. Lett. **34**(15), 2369–2371 (2009).
36. J. M. O. Daniel, J. S. P. Chan, J. W. Kim, J. K. Sahu, M. Ibsen, and W. A. Clarkson, "Novel technique for mode selection in a multimode fiber laser," Opt. Express **19**(13), 12434–12439 (2011).
37. N. Bhatia, K. C. Rustagi, and J. John, "Single LP(0,n) mode excitation in multimode fibers," Opt. Express **22**(14), 16847–16862 (2014).
38. F. Dubois, P. Emplit, and O. Hugon, "Selective mode excitation in graded-index multimode fiber by a computer-generated optical mask," Opt. Lett. **19**(7), 433–435 (1994).
39. J. Wilde, C. Schulze, R. Brüning, M. Duparré, and S. Schröter, "Selective higher order fiber mode excitation using a monolithic setup of a phase plate at fiber facet," Proc. SPIE **9343**, 2078993 (2015).
40. L. W. Luo, N. Ophir, C. P. Chen, L. H. Gabrielli, C. B. Poitras, K. Bergmen, and M. Lipson, "WDM-compatible mode-division multiplexing on a silicon chip," Nat. Commun. **5**, 3069 (2014).
41. M. Baas, G. Li, and E. Van Stryland, *Handbook of Optics Vol. IV* (Mc Graw Hill, 2010), Ch. 3.

Optics EXPRESS

42. I. Savelli, F. Desevedavy, J. C. Jules, G. Gadret, J. Fatome, B. Kibler, H. Kawashima, Y. Ohishi, and F. Smektala, "Management of OH absorption in tellurite optical fibers and related supercontinuum generation," Opt. Mater. **35**(8), 1595–1599 (2013).
43. R. Kitamura, L. Pilon, and M. Jonasz, "Optical constants of silica glass from extreme ultraviolet to far infrared at near room temperature," Appl. Opt. **46**(33), 8118–8133 (2007).
44. K. Kakihara, N. Kono, K. Saitoh, and M. Koshiba, "Full-vectorial finite element method in a cylindrical coordinate system for loss analysis of photonic wire bends," Opt. Express **14**(23), 11128–11141 (2006).
45. K.-Y. Yang, Y.-F. Chau, Y.-W. Huang, H.-Y. Yeh, and D. Ping Tsai, "Design of high birefringence and low confinement loss photonics crystal fibers with five rings hexagonal and octagonal symmetry air-holes in fiber cladding," J. Appl. Phys. **109**(9), 093103 (2011).
46. V. Finazzi, T. M. Monro, and D. J. Richardson, "Small-core silica holey fibers: nonlinearity and confinement loss trade-offs," J. Opt. Soc. Am. B **20**(7), 1427 (2003).
47. G. P. Agrawal, *Fiber Optic Communication Systems* (John Wiley & Sons, 2002), Ch. 2.
48. K. Okamoto, *Fundamental of Optical Waveguides* (Academic, 2006), Ch. 4.
49. B. E. A. Saleh and M. C. Teich, *Fundamentals of Photonics* (John Wiley & Sons, 2007), Ch. 8.
50. S. F. Mansour, E. Sayed Yousef, M. Y. Hassaan, and A. M. Emara, "The influence of oxides on the optical properties of tellurite glass," Phys. Scr. **89**(11), 115812 (2014).
51. V. Mishra, S. Pratap, R. haldar, and S. K. Varshney, "Sub-wavelength dual capillaries-assisted chalcogenide optical fibers: unusual modal properties in mid-IR (2-5 mm) spectral range," IEEE J. Sel. Top. Quantum Electron. **22**(2), 4401906 (2016).
52. S. Afshar V and T. M. Monro, "A full vectorial model for pulse propagation in emerging waveguides with subwavelength structures part I: Kerr nonlinearity," Opt. Express **17**(4), 2298–2318 (2009).
53. G. P. Agrawal, *Nonlinear Fiber Optics* (Academic, 2007), Ch. 2.
54. Q. Lin, O. J. Painter, and G. P. Agrawal, "Nonlinear optical phenomena in silicon waveguides: modeling and applications," Opt. Express **15**(25), 16604–16644 (2007).
55. C. Koos, L. Jacome, C. Poulton, J. Leuthold, and W. Freude, "Nonlinear silicon-on-insulator waveguides for all-optical signal processing," Opt. Express **15**(10), 5976–5990 (2007).
56. S. Lin and D. J. Costello, Jr., *Error Control Coding* (Pearson Prentice Hall, 2004).
57. J. M. Chavez Boggio, J. D. Marconi, and H. L. Fragnito, "Crosstalk in double-pumped fiber optics parametric amplifiers for wavelength division multiplexing systems," Opt. Commun. **259**(1), 94–103 (2006).
58. J. D. Marconi, M. L. F. Abbade, C. M. Serpa-Imbett, J. Cordoba-Ramirez, and E. A. M. Fagotto, "Broadband two-pump parametric amplifier in engineered dispersion tellurite waveguides," in *Latin America Optics and Photonics Conference*, 2016 OSA Technical Digest Series (Optical Society of America, 2016), paper LTu4A.11.

1. Introduction

Historically, there has been a growing demand for network bandwidth [1–8]. The dramatic increase in capacity (~1000 times in 10 years) provided by wavelength division multiplexing (WDM) technology and Erbium doped fiber amplifiers (EDFA) paved the road for telecommunication systems to overcome bandwidth need during the 1990s and part of the 2000s. After this period, advanced modulation formats and coherent detection associated with emerging digital signal processing (DSP) techniques allowed the aforementioned systems to support new bandwidth requirements.

However, present-day Internet services, which include high definition video streaming and games, besides potential new applications, as online medical services (for instance, personalized genetic medicine for diseases that require transmission of DNA information) [1], and the Internet of Things (IoT), with ~50 billion devices up to 2020 [1], will generate data traffic growth that will certainly exceed the current technology capacity in the next decade [4]. Considering a conservative estimation of bandwidth increase of 26% per year (~1 dB/year = 10 *log* 1.26), optical networks information traffic will grow more than 100 times throughout the two next decades. Furthermore, energy consumption and device footprint are also important issues that need to be addressed in the design of broadband-enabling equipment [9].

For these reasons, several efforts have been made to improve the optical communication systems capacity, which include: channel spectral efficiency (SE) increase [10], fibers for spatial division multiplexing (SDM) [11], fibers with very low nonlinear coefficients [12], hybrid Raman-EDFAs amplification [3] to extend the EDFA bandwidth, and improvement of reconfigurable add/drop multiplexers among others. By a rough estimation of the capacity enhancement due to such developments, the SE improvement leads to up to 5 dB (~3 times) [1, 10], the mitigation of fiber nonlinearities to 2 dB (1.6 times) [4], and the most significant

Optics EXPRESS

contribution comes from SDM, 15 dB (~30 times) [11]. Hybrid Raman-EDFA amplification has led to a 3 dB (2 times) bandwidth extension. However, if the total spectral region of high transparency of standard single mode fibers could be used (1300 to 1700 nm) there would be an 11 dB (12 times) capacity improvement as compared to the EDFAs' 4 THz (~32 nm) C-band. Such an enhancement clearly depends upon the development of new broadband optical amplifiers, but it has the interesting advantage of not requiring the replacement of fiber infrastructure.

EDFAs and Raman amplifiers provide a fixed bandwidth amplification region and the latter present the benefit of being spectrally tunable. New broadband optical amplifiers should, however, simultaneously offer frequency tunability and variable bandwidth for deployment in different communication systems. Optical parametric amplifiers (OPAs) constitute an interesting class of devices with both of these features. They are based on the four-wave mixing (FWM) effect, which depends on the third-order susceptibility of the waveguide medium material. Actually, parametric amplifiers can be realized in one-pump (1P-OPA) or two-pump (2P-OPA) configurations [13, 14]. In both cases, several numerical and/or experimental analysis indicate that such amplifiers perform broadband amplification [15–21]. However, the spectra presented in these works are obtained by tuning and amplifying one single channel over the considered frequency range. Thus, they do not take into account the influence of channel crosstalk that is very important for practical communication systems. Other reports present systemic studies of fiber based OPAs [22,23] and, interestingly, consider the degradation caused by transmitting signals over multiple OPAs [23]. Nevertheless, in these situations the observed amplification bandwidths are restricted to 3 THz. It should also be noted that OPAs based on fibers, pumped with continuous lasers, need additional circuitry to suppress stimulated Brillouin backscattering [13, 20]. A possibility to overcome this problem is to use short-length waveguides as nonlinear medium. In this approach, silicon waveguides become attractive also because their nonlinearity is orders of magnitude higher than those of optical fibers [24, 25]. However, nonlinear two-photon absorption (TPA) and free-carrier absorption (FCA) limit silicon parametric gain in the 1550 nm window and the quality of modulated signals. The performance of glass OPA waveguides, has been also investigated for single channels in [26].

In this work, an ultra-broadband 2P-OPA based on tellurite glass nano-waveguide, which could be used in integrated photonics, is proposed. The device is intended to be tunable and to present variable bandwidth, reduced footprint and good energy efficiency. It was designed using a buried-channel type waveguide with a tellurite glass core and a SiO_2 cladding, following an Archimedean spiral structure to minimize the 2P-OPA area. The dispersive parameters of the nano-waveguide were conceived to offer low ripple and ultra-broad amplification bandwidth in the optical communications window. The choice for tellurite glass relies on its good thermomechanical properties [27], high nonlinearity, and negligible undesirable effects of TPA at telecommunication wavelengths [28–30] and FCA (tellurite glass is a dielectric material). A systemic analysis, with 243 channels (56 Gbps QPSK modulation format) being amplified, in a configuration where the 2P-OPA acts as an in-line optical amplifier, is also presented. The analysis includes bit error rate (BER) results, assuming that WDM signals are repeatedly attenuated and re-amplified. All these considerations are intended to provide a first systemic evaluation performance of tellurite OPAs. In fact, to the best of our knowledge, this is the first systematic literature report on the application of tellurite glass planar waveguides for parametric amplification.

The remaining of this paper is organized as follows. In Section 2, we present a brief theoretical review of OPA fundamentals. A detailed step-by-step description of the tellurite waveguide design is approached in Section 3. Section 4 shows simulation results that allow to assess the 2P-OPA performance for the transmission of WDM signals. Scenarios where the bandwidth of WDM channels are one, two or three times the bandwidth provided by EDFAs are considered. Finally, our conclusions are described in Section 5.

Optics EXPRESS

2. Brief theoretical description of OPAs

One and two-pump OPA configurations need to satisfy a nonlinear phase-matching condition in order that the parametric process efficiently builds up along the waveguide. In the case of the 1P-OPA, the pump frequency is close to the waveguide zero-dispersion wavelength, λ_0. For 2P-OPA, pumps are disposed near symmetrically over λ_0. Because of their higher amplification bandwidth and lower ripple, in this paper, we deal only with 2P-OPAs. In this case, the nonlinear interaction between pumps and signals also generate slave signals called idlers, which are located symmetrically to the average value of the pumps wavelength.

Considering the case of a lossless waveguide, it is possible to derive, from the propagation equations of the optical signals [31], the following expression for the parametric gain:

$$G = 1 + \left(\frac{x_0 \sin \mathrm{h}\, x}{x} \right)^2, \tag{1}$$

where

$$x = x_0 \sqrt{1 - \left(\frac{\kappa}{2\gamma P_0} \right)^2}, \tag{2}$$

$x_0 = \gamma P_0 L$, γ is the nonlinear coefficient, $P_0 = 2\sqrt{P_1 P_2}$, P_1 and P_2 are the pump powers, $\kappa = \Delta\beta + \gamma(P_1 + P_2)$,

$$\Delta\beta = \beta_2(\omega_c)[\Delta\omega_s^2 - \Delta\omega_P^2] + \frac{\beta_4}{12}(\omega_c)[\Delta\omega_s^4 - \Delta\omega_P^4] + \frac{\beta_6}{360}(\omega_c)[\Delta\omega_s^6 - \Delta\omega_P^6] + \ldots.,$$

$\omega_c = \frac{(\omega_1 + \omega_2)}{2}$, ω_1 and ω_2 are the pump frequencies, $\Delta\omega_s = \omega_s - \omega_c$, ω_s is the signal frequency, $\Delta\omega_P = \omega_1 - \omega_c$ and $\beta_2(\omega_c)$, $\beta_4(\omega_c)$, $\beta_6(\omega_c)$, …, are the second-, fourth-, sixth-,… order dispersion parameters at frequency ω_c, respectively.

From Eqs. (1) and (2), it is clear that the parametric gain is maximum when the phase matching condition ($\kappa \sim 0$) is satisfied. This condition depends on the waveguide dispersion through the β_2, β_4, β_6, … parameters, which implies there are no fundamental physical constraints to the 2P-OPA gain bandwidth, such as the ones imposed by quantum transitions to EDFAs.

3. Waveguide design

The proposed waveguide is a buried-channel type, with a tellurite core and SiO_2 cladding. It follows an Archimedean spiral to minimize the device footprint. Figure 1 shows a schematic view of the waveguide. Its rectangular core cross section, 698 nm high (h) and 990 nm wide (w), was designed to maximize the parametric gain and to minimize the ripple by engineering the waveguide dispersion. This waveguide presents only two modes. We inform in advance that the higher order mode is weakly coupled to the waveguide and leaks to the cladding, because of curvature bends [32, 33] in our spiral structure. In addition to this, in the spectral range analyzed (from 1400 to 1700 nm), the higher order mode presents λ_0, at 1176 nm, for one polarization state and no λ_0 for the other. Thus, its phase matching condition is not satisfied and, therefore, the corresponding nonlinear interaction is negligible. Anyway, to prevent any influence from this higher order mode, we assume that light launched into the proposed waveguide passes through some device [32–40] that ensures only the waveguide fundamental mode is excited. For this reason, hereafter, we will treat the proposed waveguide as single mode. Since the spiral radius, R, changes along the waveguide length, it is necessary

Optics EXPRESS

to find a minimum radius that concomitantly allows for low losses and for the required waveguide dispersion.

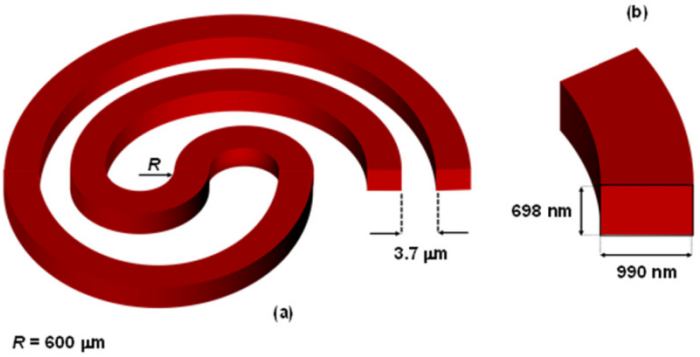

Fig. 1. a) Schematic design (not in scale) of the Archimedean spiral with their principal geometrical dimensions. b) Detail of the transversal cross sections with the high and the width of the waveguide that allow to obtain a λ_0 around 1550 nm.

The loss and the dispersion for the core and cladding materials were estimated through the following procedure. Firstly, for the core material, the refractive index was measured from a tellurite sample with composition (in mol%) 71%TeO_2– 22.5%WO_3 – 5%Na_2O – 1.5%Nb_2O_5 by using a Metricom model 2010/M prism coupling system. The experimental data were, then, fitted with a Sellmeier equation using the least square method, leading to a 0.9999 correlation coefficient. The obtained equation, which stands for the real part of the refractive index, is given by:

$$n(\lambda)=\sqrt{2.0016+2.2951\frac{\lambda^2}{\left(\lambda^2-0.046242\right)}+0.47334\frac{\lambda^2}{\left(\lambda^2-34.479\right)}}, \qquad (3)$$

and it is is plotted in Fig. 2.

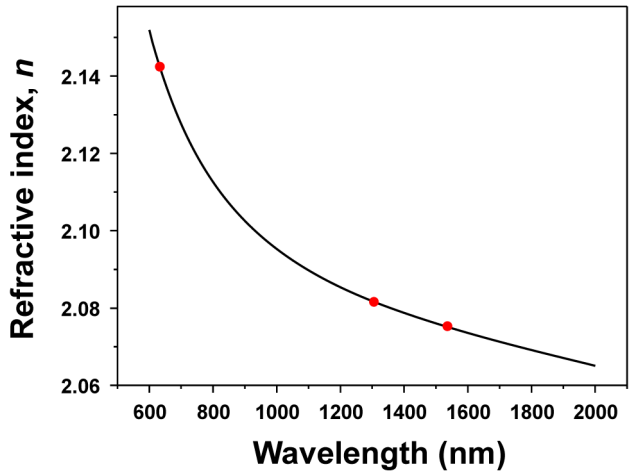

Fig. 2. Real part of tellurite refractive index as a function of wavelength. Dots are the experimental values.

The real part of the refractive index of the silica cladding was taken from [41]. The imaginary parts of the core and cladding refractive indexes were obtained from [42] and [43],

Optics EXPRESS

respectively. All these data, along with the approach given in [44] and COMSOL Multiphysics® software, were used to calculate the waveguide effective refractive index, n_{eff}. Our calculations to estimate the waveguide losses showed that the light is no longer confined for R < 70 μm, for a wavelength range from 1100 up to 1900 nm. For R > 70 μm, the confinement loss [45, 46], by considering the material losses of the core (tellurite) and the cladding (SiO_2), was calculated as a function of the wavelength and plotted in Fig. 3. From this analysis, it is evident that the minimum radius imposed by losses is R_L = 70 μm.

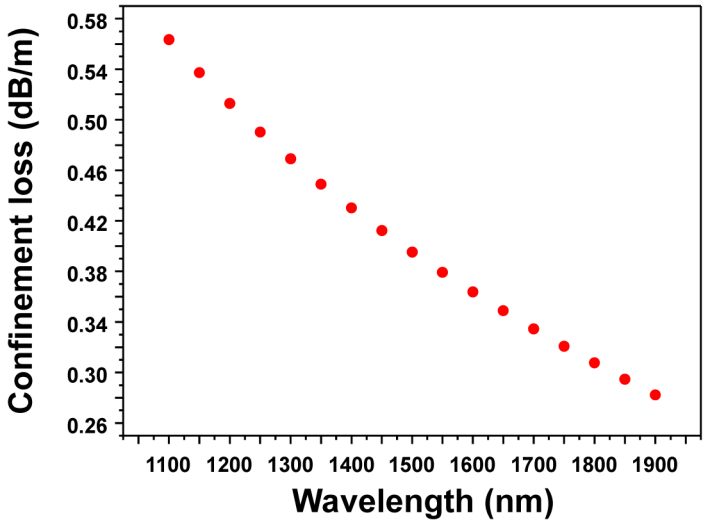

Fig. 3. Waveguide confinement losses.

Dispersion curves for the transverse electric (*TE*) (fundamental) and transverse magnetic (*TM*) modes, were calculated through the relations $\beta = k_0 n_{eff}$, $k_0 = \frac{2\pi}{\lambda}$, $\beta_2 = \frac{\partial^2 \beta}{\partial \omega^2}$, and $D = \left(-\frac{2\pi c}{\lambda^2}\right)\beta_2$ [47]. Figure 4(a) shows the dependence between dispersion and wavelength for R ranging from 30 to 800 μm, for *TE* mode. As R increases, the dispersion curves get closer to one another and there is no detectable variation for a minimum R imposed by dispersion of R_D = 500 μm. A very important feature for dispersion engineering is λ_0, whose spectral region in the considered waveguide is embraced by the two dotted vertical lines in Fig. 4(a). In Fig. 4(b), data from Fig. 4(a) are rearranged to show λ_0 as a function of R. It is seen that λ_0 increases rapidly for R < 200 μm. However, for $R > R_{\lambda 0}$, with $R_{\lambda 0}$ ~500 μm, λ_0 tends to a constant value of ~1550 nm that is very interesting for telecommunication applications. From Fig. 4(c) it is possible to observe a similar behavior for the *TM* mode, but in this case λ_0 is located at ~1400 nm.

Optics EXPRESS

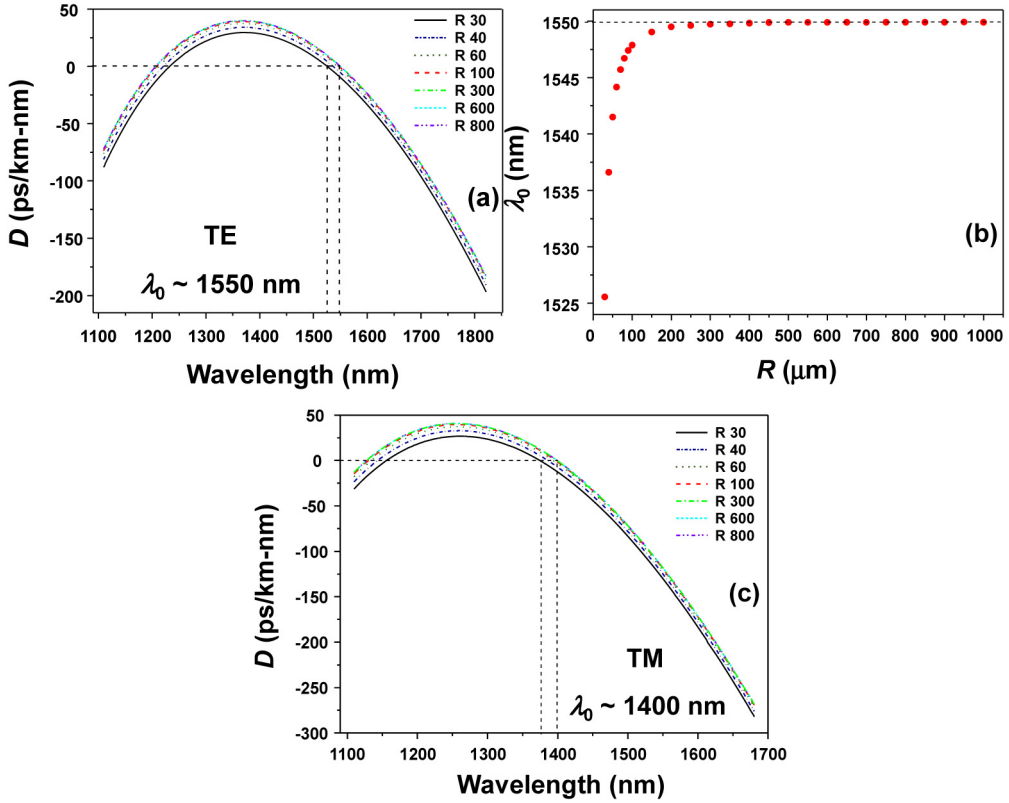

Fig. 4. a) Waveguide dispersion curves of the TE (fundamental) mode for 30 μm ≤ R ≤ 800 μm. b) ZDW as a function of the R. c) Dispersion curves of the TM mode for 30 μm ≤ R ≤ 800 μm.

The minimum radius, R_{min}, for the inner "S" of the waveguide Archimedean spiral (Fig. 1) must satisfy:

$$R_{min} \geq \max(R_L, R_D, R_{\lambda_0}), \tag{4}$$

where $\max(a_1,\ldots, a_k)$ is a function that returns the largest value among $a_1,\ldots, a_k$ and k is an integer number. Consequently, from our previous discussion, we have R_{min} = 500 μm and, as indicated in Fig. 1, we adopted R = 600 μm with a safety margin of 100 μm.

Another fundamental feature to be assessed is the coupling loss between adjacent rounds of the spiral. It is necessary to calculate the minimum gap between successive rounds in order to minimize such loss. The situation to be considered is schematized in Fig. 5. Two parallel adjacent waveguides have their edges separated by a gap Γ. Assuming that initially light is only in waveguide I (mode TE_1), there will be a propagation distance, named coupling length, L_c, after which the energy is completely transferred from waveguide I to waveguide II (mode TE_2).

Optics EXPRESS

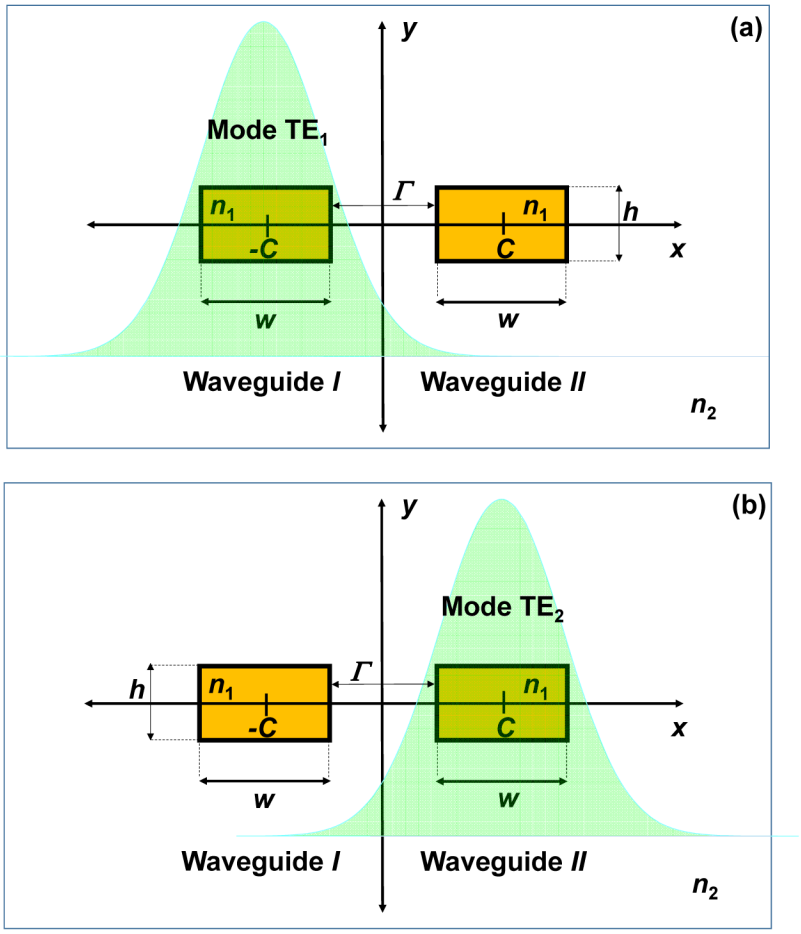

Fig. 5. a) Initially, the energy of the mode TE_1 is fully located in waveguide *I*. b) After a propagation distance equal to L_c, the energy is completely transferred to waveguide *II* (mode TE_2). The coefficients n_1 and n_2 are de refractive index of the core and the cladding, respectively.

It is possible to calculate the value of Γ that leads to $L_c >> L_s$, where L_s is the spiral length. Following the coupled-mode theory developed in [48], which considers adjacent single-mode waveguides, the coupling coefficient κ_{12}, obtained through an overlap integral between the waveguides field modes, is given by:

$$\kappa_{12} = \frac{\omega\varepsilon_0(n_1^2 - n_2^2)\int_{-h}^{+h}\int_{C-w/2}^{C+w/2}\overline{E_1^*}\,\overline{E_2}\,dxdy}{\int_{-\infty}^{+\infty}\int_{-\infty}^{+\infty}\hat{k}\cdot\left(\overline{E_1^*}\times\overline{H_1} + \overline{E_1}\times\overline{H_1^*}\right)dxdy}, \tag{5}$$

where κ_{12} is related to L_c as $L_c = \pi/(2\kappa_{12})$, ω is the angular frequency, ε_0 is the vacuum electric permittivity, n_1 and n_2 are, respectively, the core and the cladding refractive indices, and $\overrightarrow{E_1}$ and $\overrightarrow{H_1}$ are the uncoupled waveguide electric and magnetic fields related to mode TE_1 of waveguide *I*. Similarly, $\overrightarrow{E_2}$ and $\overrightarrow{H_2}$ are the uncoupled waveguide electric and magnetic fields related to mode TE_2 of waveguide *II*. The waveguide dimension parameters, *h*

Optics EXPRESS

and w, on the integral limits and the core center, C, are shown in Fig. 5. Equation (5) quantifies the coupling between TE_1 of waveguide I to TE_2 of waveguide II. The derivation of Eq. (5) assumes that the evanescent field of $\overrightarrow{E_1}$ in the region of waveguide II is considerably small. This condition is known as weak coupling and it is satisfied when the two waveguides are sufficiently separated. Under weak coupling, the spatial distributions of the modes, and their propagation constants, remain unchanged and only the field amplitudes vary [49].

Following the approach of [34] for a rectangular waveguide, the electric and magnetic fields involved in (5) are given by $\overrightarrow{E_1} = (Ex_1, Ey_1, 0)$, $\overrightarrow{E_2} = (Ex_2, Ey_2, 0)$, and $\overrightarrow{H_1} = (0, Hy_1, Hz_1)$. Furthermore, for a rectangular waveguide, we can also assume $|Ex_1| >> |Ey_1|$ and $|Ex_2| >> |Ey_2|$, leading to a coupling coefficient:

$$\kappa_{12} = \frac{\omega\varepsilon_0 (n_1^2 - n_2^2) \int_{-h}^{+h} \int_{C-w/2}^{C+w/2} Ex_1^* Ex_2 \, dxdy}{2 \int_{-\infty}^{+\infty} \int_{-\infty}^{+\infty} \Re e\left(Ex_1^* Hy_1\right) dxdy}. \quad (6)$$

Numerical results obtained for L_c as a function of Γ, for the TE mode, are presented in Fig. 6 for λ = 1750 nm. The minimum gap considered was Γ = 1.5 μm.

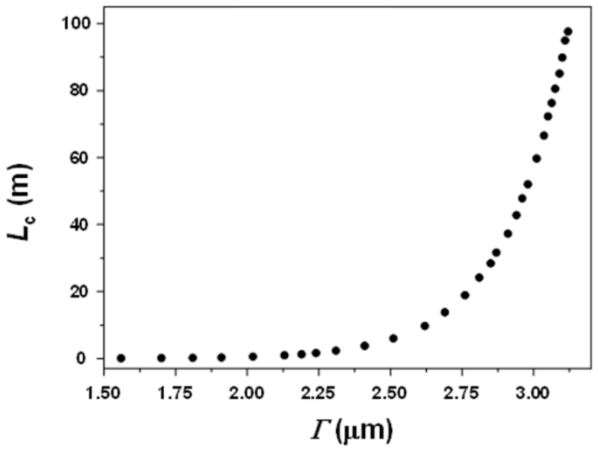

Fig. 6. Coupling length as a function of the gap width between adjacent waveguides.

In this case, as shown in Fig. 7, the magnitude of $\overrightarrow{E_1}$ is ~35 dB weaker in the region of waveguide II, which guarantees the weak coupling condition and assures the validity of Eq. (5). Longer wavelengths imply higher evanescent field magnitudes. Moreover, all of our systemic simulation results presented in Section 4 apply to wavelengths shorter than 1750 nm. Therefore, calculations for λ = 1750 nm in Fig. 7 ensure that the critical hypothesis of weak coupling holds for all of our simulations results.

Optics EXPRESS

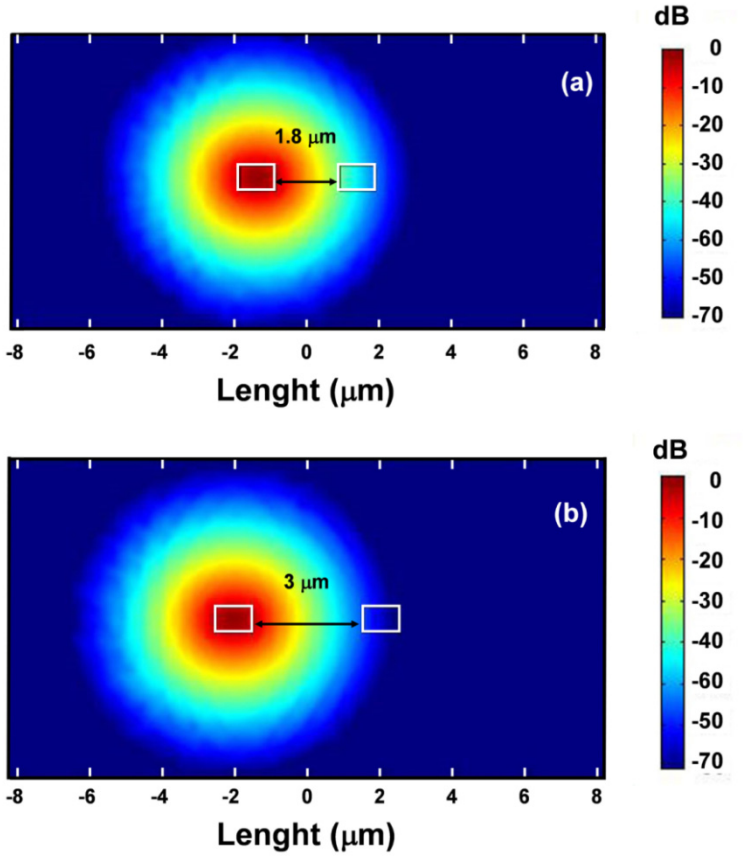

Fig. 7. a) Magnitude of the TE mode for a gap of 1.8 μm. b) 3 μm.

In order to define a limit for the minimum gap between adjacent spiral rounds, we note that for Γ ~3.1 μm, L_c ~100 m. This means that in the case of a hypothetical very long spiral, after 100 m of optical path, the optical power would be completely transferred from waveguide *I* to waveguide *II*, after 50 m only half of power would be transferred, and so on. Now, extrapolating the simulated points, it is found that, for Γ ~3.7 μm, L_c ~1 km. Considering that L_s is ~25 cm, the fraction of the optical power that will be transferred from waveguide *I* to waveguide *II*, after 25 cm of optical path, would be (L_s/L_c). 100 = 0.025% = −36 dB, which is considerably low. Then, Γ ~3.7 μm was taken as a reasonable value of the minimum gap between adjacent rounds of the spiral to allow for negligible coupling losses. This value implies the spiral should have 55 rounds to obtain L_s = 25 cm and that the outermost spiral round radius is 0.85 mm. As a consequence, the waveguide covers an area of ~2.5 mm^2.

This Γ ~3.7 μm value is a consequence of the high confinement of the fundamental *TE* mode as shown in Fig. 7. The color scale in dB indicates the modulus of the electric field for waveguide *I*. For a gap of 1.8 μm, the electric field from waveguide *I* drops ~45 dB in the region of waveguide II (Fig. 7(a)). The difference increases to ~60 dB or more for a gap of 3 μm (Fig. 7(b)).

Finally, considering an effective cross section area of ~0.7 μm^2 and a nonlinear refractive index n_2 ~$5 \cdot 10^{-19} m^2/W$ [50], the waveguide nonlinear parameter, as defined in [47], can be estimated as γ ~3000 W^{-1} km^{-1}. A more sophisticated approach would include the influence of the longitudinal component of the guided modes to compute γ [51, 52]. However, for the contrast index, waveguide dimensions, and spectral range considered in the simulations of the

Optics EXPRESS

next section, the correction introduced by such approach should be relatively small as can be estimated from Fig. 5 of [52]. Under these conditions, it would only slightly increase our estimation of γ, which would lead to marginally lower pump powers to operate the OPA, with no significant change on the discussed waveguide properties.

4. 2P-OPA performance

The mathematical dependence between parametric gain and phase matching condition was pointed out in Section 2. In the present section, the use of the designed waveguide as a gain medium for a two-pump parametric amplifier (2P-OPA) is assessed. The nonlinear Schrödinger Equation (NLSE) properly describes the propagation of optical fields through the longitudinal direction of waveguides [53–55]. In order to simulate the performance of the proposed 2P-OPA we used VPItransmissionMaker software. In particular, a VPItransmissionMaker module, set with our engineered dispersion, was used to solve the NLSE through the split-step Fourier method. A constant waveguide attenuation of 0.5 dB/m was utilized. This value corresponds to the largest loss observed in the spectral range of interest for our simulations (Fig. 3). In accordance with our previous discussion, the nonlinear parameter was set to 3000 $(W \cdot km)^{-1}$. All signal channels were simulated with a pseudo-random bit sequence (PRBS) of length 2^{12}-1. A typical spectrum gain is shown in Fig. 8. The pumps were tuned at λ_{P1} = 1411.65 nm and λ_{P2} = 1687.7 nm (separation of 276 nm) with powers $P_{P1} = P_{P2}$ = 33 dBm, where P_{Pi} stands for the power of the pump placed at λ_{Pi} (i = 1, 2). A set of 243 input single polarization 56 Gbps quadrature phase shift keying (QPSK) modulated signal channels was placed from 1544.917 nm up to 1647.204 nm within the 50 GHz grid. The gain was ~16 dB with a ripple of ~4.5 dB, over a bandwidth of ~102 nm (12 THz), which is 3 times larger than the one obtained with C band EDFAs. The 2P-OPA optical signal-to-noise ratio (OSNR) was estimated by using the following procedure: (i) A given signal channel power was measured; (ii) Afterwards, the signal was suppressed and, then, at its frequency, the noise background power was measured; (iii) The 2P-OPA OSNR is just the ratio between these measurements, that is, 13.4 dB.

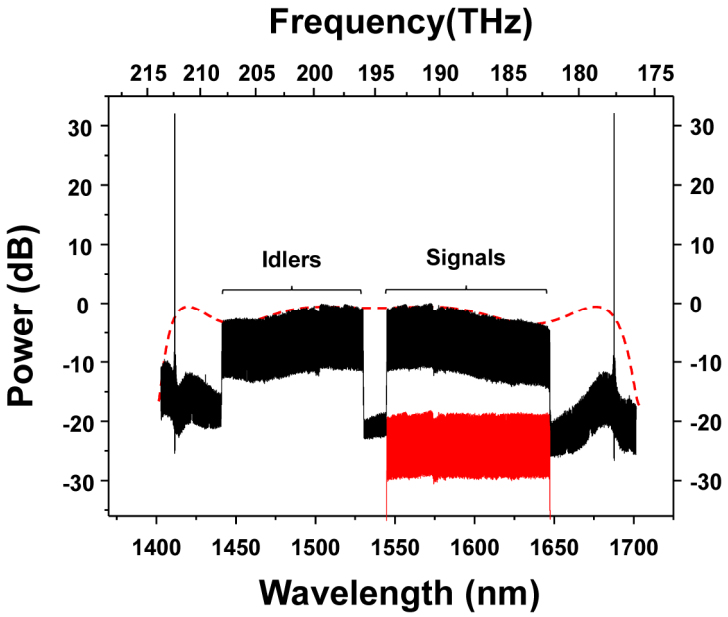

Fig. 8. 2P-OPA gain spectrum obtained for the designed waveguide. The dotted red line is the OPA gain obtained with the analytic model. The continuous red line is the OPA input set of channels.

Optics EXPRESS

Figure 8 also shows the gain spectra obtained with the analytic model presented in Section 2, with the same pump parameters used to solve the NLSE. The agreement between them is rather good. This fact is important because it clearly shows that some of the characteristics that determine the performance of the parametric amplifier, as gain, ripple and bandwidth, depend essentially on the phase matching condition, which relies on the dispersive properties of the waveguide. For instance, to calculate the analytic gain spectra, $\beta_2(\omega_c)$ can be written as $\beta_2(\omega_c) = \beta_3(\omega_c)\ (\omega_c - \omega_0) + \beta_4(\omega_c)\ (\omega_c - \omega_0)^2/2$, where $\omega_0 = (2\pi\ c)/\lambda_0$ and $\omega_c = ((\omega_1 + \omega_2)\ /2)$ (ω_1 and ω_2 are the pumps frequencies). This shows certain high-order dispersion parameters have a fundamental role for engineering the dispersion. The curves for $\beta_2(\omega)$, $\beta_3(\omega)$ and $\beta_4(\omega)$, the two last obtained through the derivatives of the $\beta_2(\omega)$, are shown in Fig. 9 (these curves were presented as a function of λ for sake of clarity). The values at $\lambda_c = (2\pi\ c)/\omega_c = 1537.34$ nm are $\beta_3(\lambda_c) = -0.67$ ps^3/km and $\beta_4(\lambda_c) = 0.007$ ps^4/km. The sixth order dispersion parameter is $\beta_6(\lambda_c) = 3.26\ 10^{-7}$ ps^6/km. Such a value is small enough to neglect the β_6 term in the expansion of $\Delta\beta$ ($\left|[(\beta_6(\omega_c)/360)[\Delta\omega_s^6 - \Delta\omega_P^6]/(\beta_4(\omega_c)/12)[\Delta\omega_s^4 - \Delta\omega_P^4]\right| \sim 10^{-2}$), and, furthermore, it has no significant effect on the parametric gain. The analytic curve, which takes into account only the contributions of $\beta_2(\omega)$, $\beta_3(\omega)$ and $\beta_4(\omega)$, matches quite well the spectral gain obtained by solving the NLSE. This allowed us to verify that the small spectral ripple obtained is a consequence of the positive values of $\beta_4(\omega)$ [14].

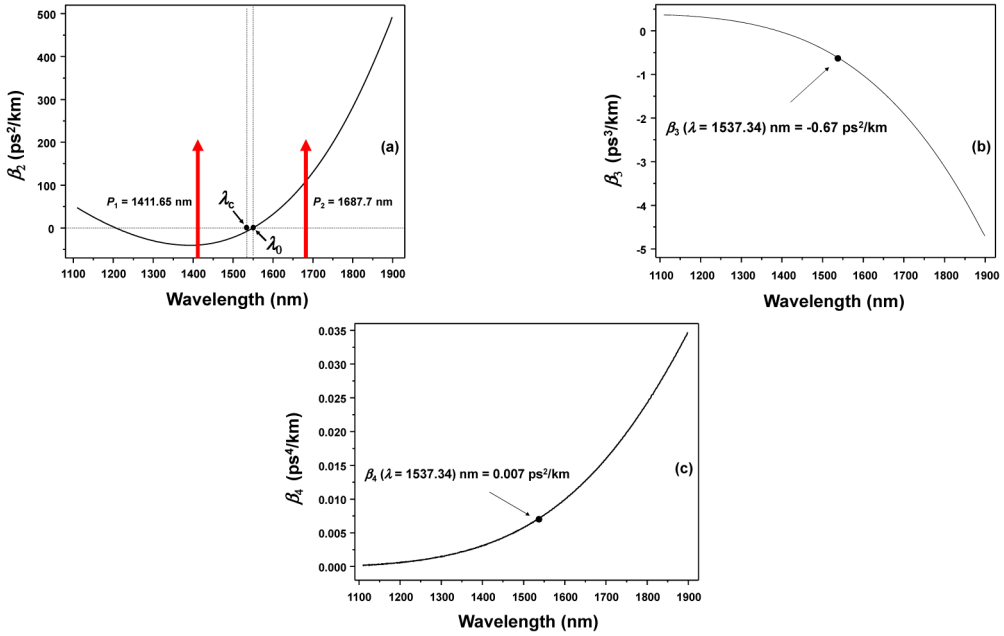

Fig. 9. Curves for: a) $\beta_2(\lambda)$. The red arrows show the pumps positions, and the black points the position of λ_c and λ_0. b) $\beta_3(\lambda)$. c) $\beta_4(\lambda)$. Dots indicate the values of $\beta_3(\lambda_c) = -0.67$ ps^3/km and $\beta_4(\lambda_c) = 0.007$ ps^4/km for $\lambda_c = 1537.34$ nm.

Figure 10 exhibits the bit error rates (BER) for 13, from 243 channels, spaced by ~1 THz. Firstly, the modulated channels with a power of ~-18 dBm were passed a single time by the 2P-OPA under consideration. At the amplifier output, the BERs were below 10^{-8} (Fig. 10(a)) and the signal power was around −1.5 dBm. Afterwards, we simulated a scenario where all signals were equalized and transmitted through consecutive 80-km-long spans of standard fiber, with an attenuation of ~0.18 dB/km, followed by a 2P-OPA. Since we are concerned with the amplifier performance, we assumed that the dispersion induced by the fiber spans was exactly compensated before the 2P-OPA. The curves in Fig. 10(a) show that after the

Optics EXPRESS

sixth pass through the 2P-OPA, the BER is about ~10^{-2}, which can be turned into 10^{-15} by using forward error correction (FEC) mechanisms [56]. This propagation distance is compatible with the scale length of metropolitan area networks (MANs). For illustrative purposes, Fig. 10(b) shows the constellation diagrams for the best and the worst BER cases, after the first and the sixth passes. Under the considered simulation conditions, BER degradation is related to optical signal to noise ratio (OSNR) reduction and to the crosstalk that is inherent to parametric amplification [57]. The output spectrum at the sixth span output is shown in Fig. 11. After the sixth-pass, the OSNR is degraded by ~2.7 dB if compared to the first-pass.

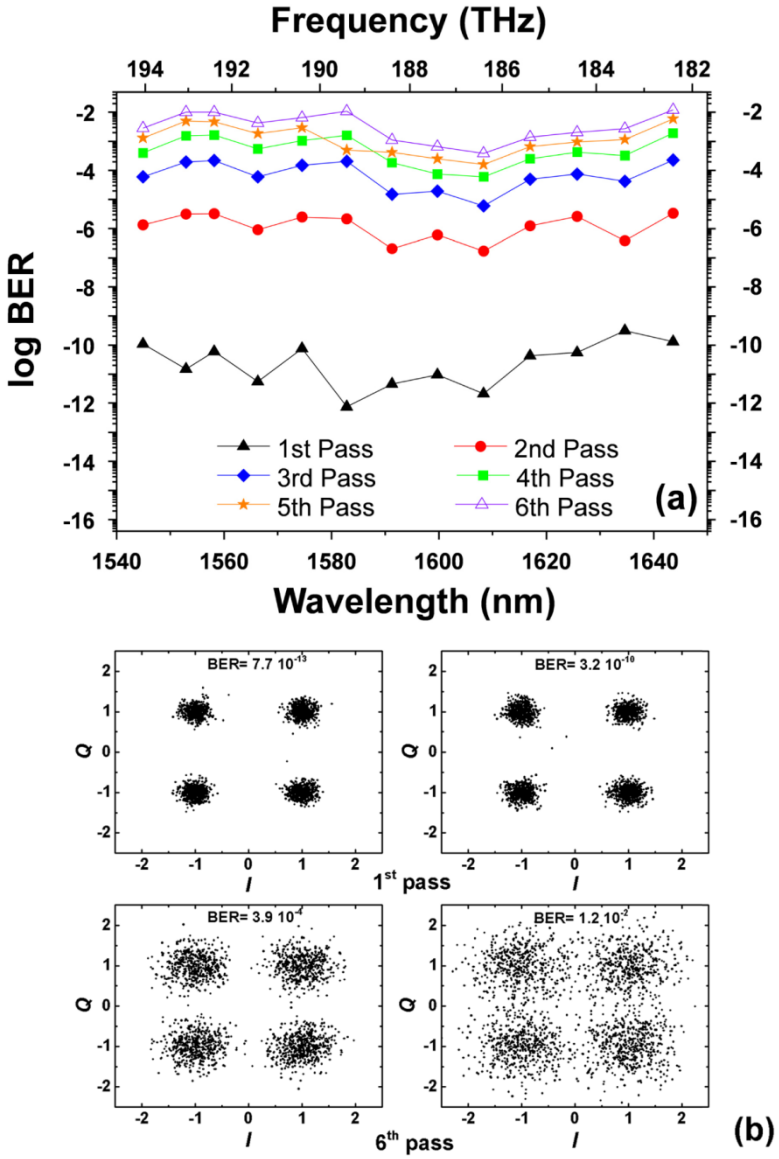

Fig. 10. a) BER performance for a 2P-OPA based on the designed tellurite waveguide. b) Constellation diagrams in the best and the worst BERs cases, for the 1st and the 6th passes.

Optics EXPRESS

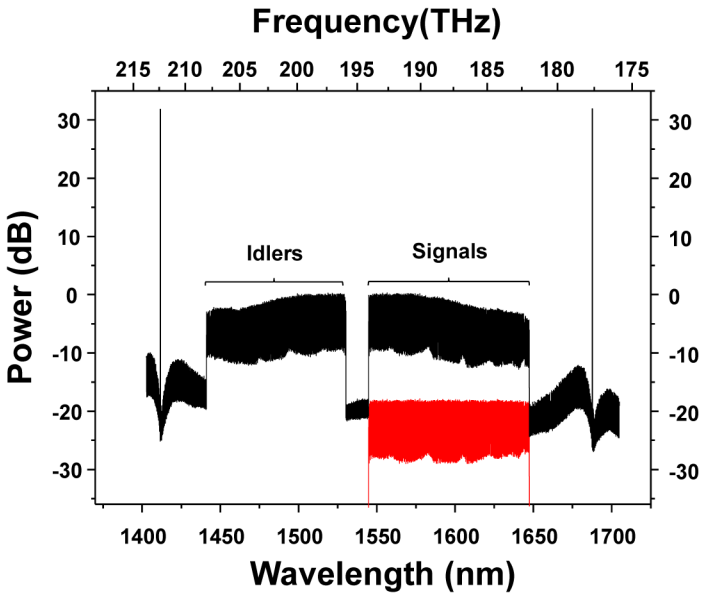

Fig. 11. Gain spectrum at the output of the sixth span of standard fiber followed by the sixth 2P-OPA. The continuous red line is the OPA input set of channels.

We also evaluated the 2P-OPA performance for 180 (9 THz or ~77.3 nm, as pointed out in our preliminary results [58])) and 100 (5 THz or ~43.9 nm) channels. In both cases, BERs were very low (below 10^{-16}) after the first pass and, thus, they can be considered error-free. Figure 12 shows a BER comparison for the case when signals underwent a second pass. Even in this situation, the BER values for 100 channels remain below 10^{-16}.

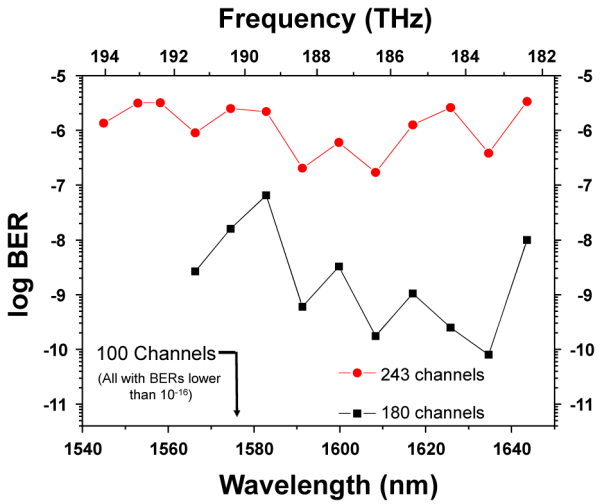

Fig. 12. 2P-OPA BER performance for different number of amplified 56 Gbps QPSK signals, spaced by 50 GHz.

These results are in agreement with previous findings that show how the crosstalk in 2P-OPAs increases with the number of amplified channels [57]. Such a crosstalk could be reduced by shortening the waveguide length and by increasing the pumps power or by manipulating the dispersive properties to minimize the spurious four-wave mixing products and other crosstalk mechanisms.

Optics EXPRESS

Therefore, our results suggest that the designed parametric amplifier may be used in networks with diameters larger than those of MANs, where the number of amplified channels is up to two times the one covered by conventional EDFAs. Alternatively, the device could be used for network with larger diameters if the number of channels could be reduced.

Currently, deployed commercial 100 Gbps WDM systems transmit 56 Gbps QPSK signals in two orthogonal polarizations. The analysis presented in this work is valid for one of such polarizations. A second amplifier or some polarization diversity scheme would be necessary to take the second polarization into account.

5. Conclusions

An ultra-broadband (~102 nm), low-ripple (~4.5 dB), small footprint (~2.5 mm^2), two-pump-optical parametric amplifier (2P-OPA) that employs a tellurite glass buried-channel type waveguide as nonlinear medium was numerically designed and investigated. This device is tunable and it can also be adjusted to exchange bandwidth by reach. The proposed waveguide was designed in an Archimedean spiral geometry to minimize the device footprint. For the dispersion calculations, the tellurite refractive index was obtained by fitting experimental data with a Sellmeier equation. The waveguide losses were of 0.5 dB/m and a 3.7 μm minimum gap between adjacent rounds of the spiral was adopted to keep coupling losses lower than 0.025%. Its nonlinear parameter was estimated as γ ~3000 W^{-1} km^{-1}, for a nonlinear refractive index n_2 ~5 x $10^{-19}m^2/W$ and an effective area of ~0.7 μm^2.

From an application point of view, our results suggest that the designed waveguide could amplify 243 QPSK 56 Gbps signals, spaced by 50 GHz, with an average gain of ~16 dB. The resulting amplification bandwidth is ~3 times larger than the one provided by C-band EDFAs, whereas a ripple of 4.5 dB is approximately the same. Results also suggest that signals could be propagated by around $6 \cdot 80$ km = 480 km, which correspond to a relatively large optical MAN. Longer reaches could be achieved by using DSP techniques to mitigate the influence of nonlinear crosstalk or by reducing the number of amplified channels.

In conclusion, the designed tellurite waveguide seems to be a very attractive medium for the realization of 2P-OPAs, which may become key devices for the development of the next generation of core networks. In fact, thanks to the OPAs tunability, four unities of the investigated device could be used in parallel to cover all the spectral region of SMF high transparency (1300 to 1700 nm) and to provide the 11 dB capacity improvement mentioned in Section 1, for MAN applications. A lower number of parallel 2P-OPAs could be used, if the waveguide dispersion is further engineered to reduce channel crosstalk or if DSP techniques are deployed to mitigate such effects. Furthermore, because of the tellurite glass high transparency and nonlinearity, thermal stability, and non-susceptibility to FCA and TPA, they have very strong potential for the development of photonic integrated circuits to be used in future optical communication systems.

Funding

Conselho Nacional de Pesquisa e Desenvolvimento (CNPq) (311137/2014-8, 311870/2014-7); Program INCT/FOTONICOM (CNPq 574017/2008-9 and FAPESP 2008/57857-2).

Acknowledgments

The Authors would like to thank Eng. Gabriel J. Suzigan for important discussions and VPIphotonics for providing academic licenses of the simulation software tools utilized in this work. We also like to express our deepest gratitude to Prof. H. L. Fragnito for providing access to Optical Communications Laboratory facilities at IFGW-UNICAMP.